Inorganic Chemistry
Article

Inorg. Chem. **2010**, *49*, 5515–5521 **5515**
DOI: 10.1021/ic100249t

Tunable Aqueous Phase Synthesis and Shape-Dependent Electrochemical Properties of Rhodium Nanostructures

Qiang Yuan,[†,‡] Zhiyou Zhou,[*,§] Jing Zhuang,[†] and Xun Wang[*,†]

[†]*Department of Chemistry, Tsinghua University, Beijing 100084, P. R. China,* [‡]*Department of Chemistry, Guizhou University, Guiyang, Guizhou province 550025, P. R. China, and* [§]*Department of Chemistry, College of Chemistry and Chemical Engineering, Xiamen University, Xiamen, 361005, P. R. China*

Received February 6, 2010

Rhodium nanostructures with highly selective morphologies such as cubes, horned particles, dendrites, and network-shaped wires have been achieved through the synergetic effect of sodium lauryl sulfate (SLS) and halogen anions (F^-, Cl^-, Br^-, I^-) in a green solvent, water. The effects of SLS and halogen anions were systematically investigated. The electrocatalytic performances of Rh nanostructures toward ethanol oxidation were tested. The results have shown that the rhodium nanostructures displayed shape-dependent properties, and the nanodendrites possessed the maximum catalytic activity.

Introduction

The synthesis of noble metal nanocrystals with controllable morphologies (including dimension and shape) has received increasing interest because of the nanocrystals' intrinsic shape- and size-dependent properties in many key fields such as catalysis,[1−6] biotechnology,[7] magnetism,[8] and optics.[1,9] Noble metal nanocrystals with a variety of morphologies including a sphere, polyhedron, plate, wire, dendrite, and so forth have been synthesized by the bottom-up, solution-phase methods. Meanwhile, up to now, the solution systems, which were developed to control the crystal morphology of noble metal, mainly focused on polyol, oil, and other organic solvent systems.[7,10,11] The morphology-controllable synthesis of single noble metal nanocrystals in a "green" solvent such as water still remains a challenge. In this paper, we demonstrate rhodium as a case study in which the morphology of rhodium nanocrystals can be harnessed in the aqueous phase through the synergetic effect of SLS and different halogen anions while maintaining other reaction conditions (Figure 1). Moreover, the electrocatalytic activity of Rh nanostructures toward ethanol oxidation exhibits shape-dependent properties.

Rhodium is a very important catalyst in many industrial and lab applications. For example, rhodium is a well-known catalyst for NO_x reduction in three-way car catalysts,[12] direct ethanol fuel cells (DEFCs),[13] oxidation of alcohols into organic acids,[14] hydrogenation/hydroformylation of unsaturated hydrocarbon compounds,[15] and in the petroleum refining process.[16] On the other hand, the price of rhodium is very high. Therefore, for the sake of maximum utilization of rhodium, it is necessary to precisely control the size and shape of rhodium crystals for exposing the maximum number of atoms.

For the above-mentioned reasons, much effort to synthesize monodispersed, well-defined rhodium nanostructures with high selectivity has been expended in the solution system. However, limited success has been achieved for controlling the morphology of rhodium compared to other noble metals (Ag, Au, Pd, and Pt). In 2005, Tilley and co-workers first

*To whom correspondence should be addressed. E-mail: zhouzy@xmu.edu.cn (Z.Z.), wangxun@mail.tsinghua.edu.cn (X.W.).

(1) Xia, Y. N.; Xiong, Y. J.; Lim, B.; Skrabalak, S. E. *Angew. Chem., Int. Ed.* **2009**, *48*, 60.
(2) Lee, H.; Habas, S. E.; Kweskin, S.; Butcher, D.; Somorjai, G. A.; Yang, P. D. *Angew. Chem., Int. Ed.* **2006**, *46*, 7824.
(3) Park, J. Y.; Zhang, Y. W.; Grass, M.; Zhang, T. F.; Somorjai, G. A. *Nano Lett.* **2008**, *8*, 673.
(4) Wang, C.; Daimon, H.; Onodera, T.; Koda, T.; Sun, S. *Angew. Chem., Int. Ed.* **2008**, *47*, 3588.
(5) Tian, N.; Zhou, Z. Y.; Sun, S. G.; Ding, Y.; Wang, Z. L. *Science* **2007**, *316*, 732.
(6) Ming, T.; Feng, W.; Tang, Q.; Wang, F. G.; Sun, L.; Wang, J.; Yan, C. *J. Am. Chem. Soc.* **2009**, *131*, 16350.
(7) Ferrando, R.; Jellinek, J.; Johnston, R. L. *Chem. Rev.* **2008**, *108*, 845.
(8) Cademartiri, L.; Ozin, G. *Adv. Mater.* **2009**, *21*, 1013.
(9) Zhang, Q.; Ge, J.; Pham, T.; Goebl, J.; Hu, Y.; Lu, Z.; Yin, Y. D. *Angew. Chem., Int. Ed.* **2009**, *48*, 3516.
(10) Dumestre, F.; Chaudret, B.; Amiens, C.; Renaud, P.; Fejes, P. *Science* **2004**, *303*, 821.
(11) Huang, X.; Zhang, H.; Guo, C.; Zhou, Z.; Zheng, N. *Angew. Chem., Int. Ed.* **2009**, *48*, 4808.
(12) Gandhi, H. S.; Graham, G. W.; McCabe, R. W. *J. Catal.* **2003**, *216*, 433.
(13) Kowal, A.; Li, S. M.; Sasaki, K.; Vukmirovic, M. B.; Zhang, J.; Marinkovic, N. S.; Liu, P.; Frenkel, A. I.; Adzic, R. R. *Nat. Mater.* **2009**, *8*, 325.
(14) Fujita, M.; Hiyama, T. *Org. Synth. Coll.* **1993**, *8*, 16.
(15) Park, K. H.; Jang, K.; Kim, H. J.; Son, S. U. *Angew. Chem., Int. Ed.* **2007**, *46*, 1152.
(16) Akao, A.; Sato, K.; Nonoyama, N.; Mase, T.; Yasuda, N. *Tetrahedron Lett.* **2006**, *47*, 969.

Published on Web 05/25/2010

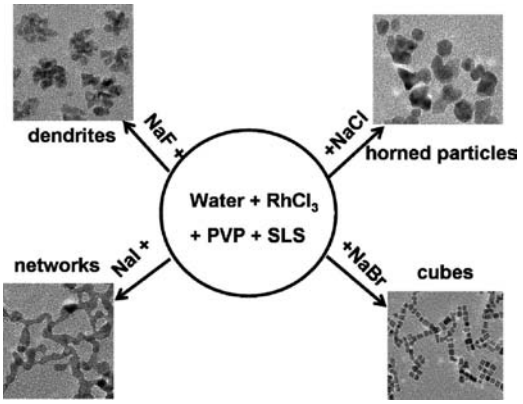

Figure 1. Summary of Rh nanostructures controlled by halogen anions.

synthesized the high-yield rhodium nanocubes and multipods by reducing $RhCl_3$ in the ethylene glycol−poly(vinylpyrrolidone) (PVP) system using the seed growth method by manipulating the temperature.[17] Xia and co-workers also reported rhodium tripods/tetrapods with anhydrous Na_3RhCl_6 as a precursor in the ethylene glycol−PVP system.[18] Son and co-workers obtained high-yield rhodium tetrahedrons to decompose the organometallic compound, $[Rh_2(CO)_4Cl_2]$, in oleylamine.[15] Somorjai and co-workers achieved rhodium nanocubes with >85% selectivity in the ethylene glycol−PVP−TTAB (trimethyl(tetradecyl)ammonium bromide) system with $RhCl_3$ hydrate as a precursor.[19] However, the other novel rhodium nanostructures such as dendrites and network-shaped wires have not been reported thus far. In this paper, rhodium nanostructures with highly selective morphologies such as cubes, horned particles, dendrites, and network-shaped wires have been synthesized (Figure 1). Moreover, the electrocatalysis activity of Rh nanostructures toward ethanol oxidation exhibits shape-dependent properties.

Experimental Section

Chemicals. Poly(vinylpyrrolidone) (PVP; CP, MW = 30 000), NaF (A.R.), NaCl (A.R.), NaBr (A.R.), NaI (A.R.), sodium lauryl sulfate (SLS; A.R.), and ethanol (99.99%) were purchased from Beijing Chemical Reagent Company. $RhCl_3 \cdot nH_2O$ (A.R., Rh content: 40 wt %) was purchased from the Beijing Research Institute for Nonferrous Metals. $HClO_4$ were purchased from Alfa Aesar. Chemicals were used as received without further purification. Deionized water was used for the synthesis of nanocrystals.

Synthesis of Rh Nanodendrites and Other Morphology Crystals. A total of 1.0 mL of $RhCl_3$ (0.1 M) aqueous solution, 21.0 mg of NaF (0.5 mmol), 300 mg of PVP (MW = 30 000), and 289 mg of SLS were added to 7.0 mL of water and stirred for 5 min. The resulting homogeneous brown solution was transferred to a 12 mL Teflon-lined stainless-steel autoclave. The sealed vessel was then heated at 220 °C for the desired time (i.e., 1.5, 3.0, 6.0, 12, and 24 h) before it was cooled to room temperature. The products were separated via centrifugation at 10 000 rpm for 20 min three times using deionized water. Then, the products were dispersed with 5.0 mL of deionized water. The other morphologies of rhodium were obtained using the same process but, instead of NaF, with equal molar amounts of NaCl, NaBr, and NaI for 6 h.

Characterizations. The size and morphology of the nanocrystals were determined by a Tecnai G2 F20 S-Twin high-resolution transmission electron microscope (HRTEM) at 200 kV. The rhodium nanocrystal solution was deposited onto the carbon supported copper grid with a pipettor, and the solvent was allowed to evaporate for TEM detection. X-ray diffraction (XRD) patterns of the samples were recorded on a Rigaku D/max-2400 diffractometer operated at 40 kV and a 200 mA current with Cu Kα radiation (λ = 1.5418 Å). The rhodium nanocrystal solution was deposited onto the glass plate with a pipettor, and the solvent was allowed to evaporate for XRD detection. FTIR spectroscopy was performed on a Nicolet 560 spectrograph.

Test of Electrocatalytic Activity. Electrochemical experiments were carried out in a standard three-electrode cell at room temperature (about 25 °C) controlled by a PAR 263A potentiostat/galvanostat (EG&G). A saturated calomel electrode (SCE) and a platinum foil were used as the reference and counter electrodes, respectively. All potentials reported in this paper are referred to the SCE scale. The superpure water (18 MΩ cm) purified through a Milli-Q Lab system (Nihon Millipore Ltd.) was used as a solvent.

The original samples of PVP-capped Rh nanoparticles were washed several times with superpure water. Finally, 10 μL of the suspension of purified Rh nanoparticles was drop-cast onto a well-polished glassy carbon (GC, ϕ = 5 mm; Takai Carbon Co., Ltd., Tokyo, Japan) electrode and dried under an infrared lamp, to get the working electrode.

The cyclic voltammograms (CVs) were obtained in a nitrogen-saturated 0.1 M HClO4 solution, and the potential was scanned from −0.28 to 1.0 V (SCE) at a scan rate of 50 mV/s. Voltammetric measurment for ethanol oxidation was carried out in a 0.1 M ethanol + 0.1 M HClO4 solution, and the potential was scanned from −0.28 to 1.0 V (SCE) at a scan rate of 5.0 mV/s.

Results and discussion

Rhodium Nanodendrites. The typical rhodium nanodendrites were synthesized in an aqueous solution in the presence of $RhCl_3$, PVP, SLS, and NaF at 220 °C for 6 h. Figure 2a and b show the representative TEM images of as-synthesized Rh nanodendrites, indicating that the products were made of uniform nanodendrites, and no significant amounts of other morphologies were detected by TEM. The sizes of the nanodendrites have a narrow distribution from 18 to 25 nm. Meanwhile, the HAADF-STEM image (Figure 2c) reveals that the nanodendrites consist of many branches; each branch is along different a direction, and the maximum number of branches can be beyond 20. The HRTEM image (Figure 2d) shows each branch of a single rhodium nanodendrite is of a rice shape with a sharp tip and an edge-to-edge width W of about 4.8 nm, and an apex-to-apex length L around 7.3 nm. The interval between two lattice fringes was examined to be 0.220 nm, closed to the (111) lattice spacing of the fcc rhodium. Moreover, the lattice fringes of each branch are along the same direction, which indicates that the branch is single crystalline. The X-ray diffraction (XRD) pattern (Figure 2a, inset) of as-synthesized products possessed four peaks in the range of 30−90° corresponding to (111), (200), (220), and (311) planes of fcc rhodium (JCPDS 88−2334).

To achieve insight into the formation mechanism of rhodium nanodendrites, the effects of SLS and NaF were also studied. The products in the absence of SLS and NaF are displayed in Figure 3a. It shows that the products

(17) Hoefelmeyer, J. D.; Niesz, K.; Somorjai, G. A.; Tilley, T. D. *Nano Lett*. **2005**, *5*, 435.
(18) Zettsu, N.; McLellan, J. M.; Wiley, B.; Yin, Y.; Li, Z.; Xia, Y. *Angew. Chem., Int. Ed.* **2006**, *45*, 1288.
(19) Zhang, Y.; Grass, M. E.; Kuhn, J. N.; Tao, F.; Habas, S. E.; Huang, W.; Yang, P.; Somorjai, G. A. *J. Am. Chem. Soc*. **2008**, *130*, 5868.

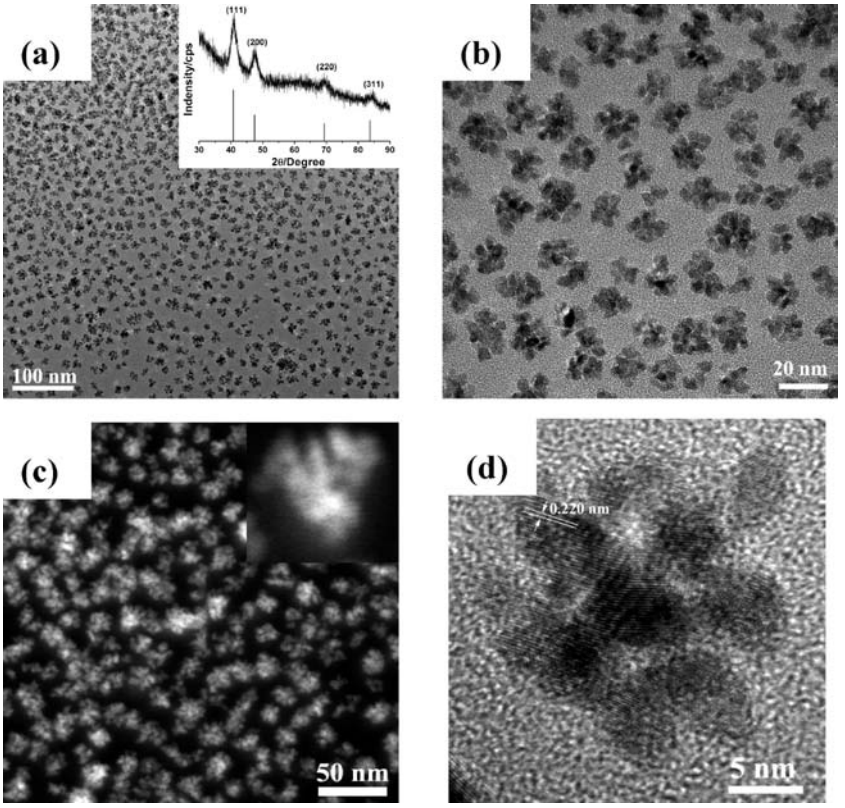

Figure 2. Representative TEM and HRTEM (a, b, and d) images of Rh nanodendrites synthesized at 220 °C for 6 h, the high-angle annular dark field (HAADF)-STEM image (c), and XRD profile of as-synthesized products (a, inset).

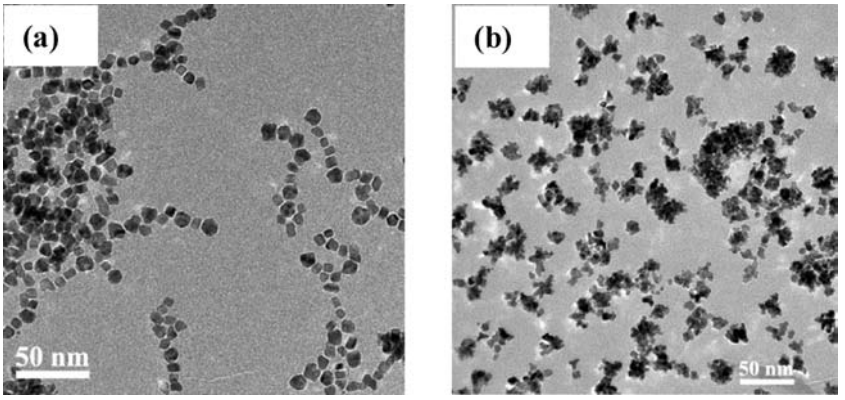

Figure 3. TEM images of Rh particles synthesized without SLS and NaF (a), and without NaF (b).

consist of monodispersed mixtures of polyhedrons with an average diameter of 8.5 ± 0.3 nm such as cubes, tetrahedra, decanedra, and so on. It indicates that PVP plays the role of a reducing and stabilizing agent, while SLS and NaF may assist the formation of the nanodendrites.[1] The FTIR spectra taken from representative rhodium dendrites, PVP, and SLS showed the PVP was on the surface of rhodium particles (Figure S1, Supporting Information) while SLS was almost negligible. When SLS was added into the reaction solution, the products consisted of ill-defined particles with uncontrollable size (Figure 3b). It is interesting that no products can be obtained in the absence of SLS while the solution contained NaF, PVP, and $RhCl_3$. These results clearly imply that the SLS and NaF can tune the nuclei and growth rate of Rh crystals with a synergetic effect.

The products obtained by varying the reaction time often contribute to an understanding of shape evolution. The TEM and HRTEM images of Rh nanodendrites obtained at different reaction times (from 1.5 to 24 h) are shown in Figure 4. It shows that the Rh nanodendrites have formed at 1.5 h (Figure 4a). However, the number of branches of particle is relatively less than that obtained at 6 h. The branches of the majority particles are not beyond 10. And the distribution of particle sizes is not uniform, being below 15.0 nm. Moreover, there are a lot of fine rhodium grains with a size below 2.0 nm (Figure 4a inset, in the white dashed circle). With an increase in reaction time, the fine rhodium grains disappeared and the size of rhodium dendrites became bigger and more uniform (Figure 4b). When the reaction time increased to 12 and 24 h, the size and uniformity of rhodium dendrites was

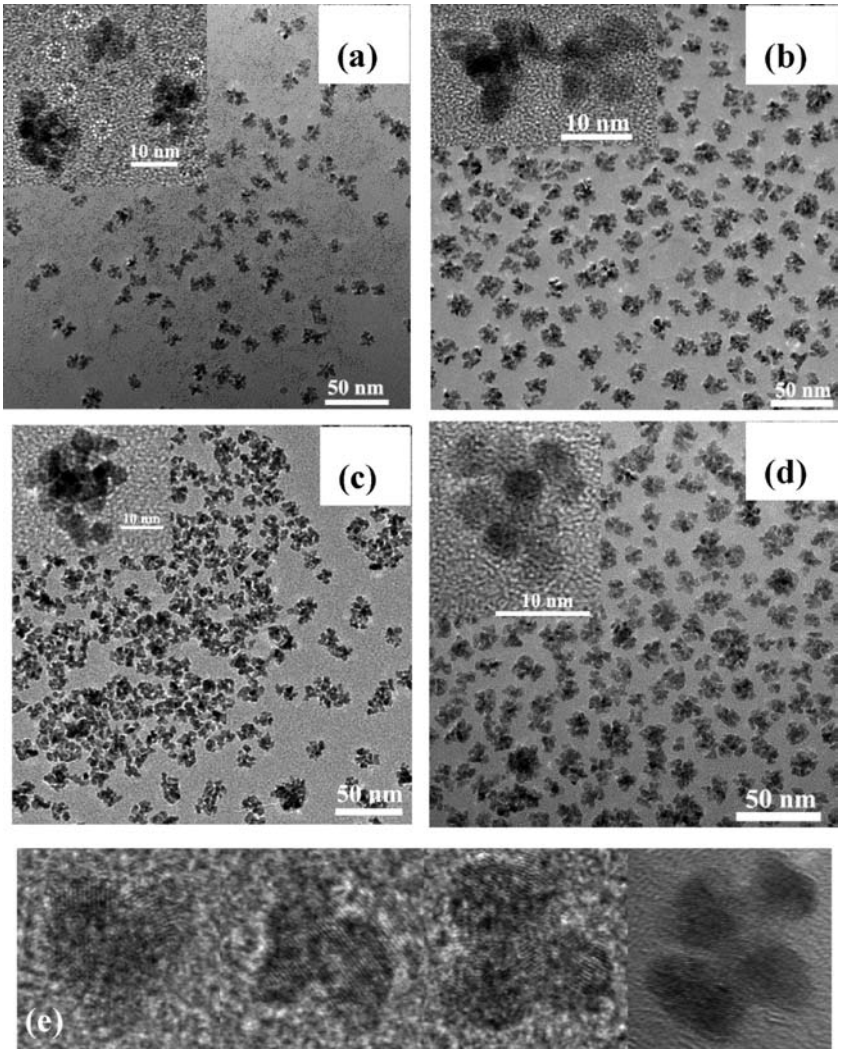

Figure 4. TEM images of Rh nanodendrites synthesized at different time. (a) 1.5 h; (b) 3 h; (c) 12 h and (d) 24 h. the insets are the corresponding HRTEM images. (e) The TEM images of intermediates of Rh nanodendrites at primary growth stage.

almost unchanged (Figure 4c and d). But the shape of branch in the dendrites evolved from a rice shape with sharp tips to spheres, owing to the minimization of the total surface energy (Figure 4c and d, inset).

The overgrowth and self-catalysis process are often used to deduce the formation mechanism of branched nanostructures.[18,20] In our synthetic system, for understanding the formation mechanism of rhodium nanodedrites, the TEM images of primary growth stages of rhodium nanodedrites were captured, including the monomer, dimer, trimer, and tetramer (Figure 4 e), which indirectly indicated that the formation of dendritic structures of rhodium particles underwent different stages. On the basis of the above-mentioned results, we deduced the possible formation mechanism of rhodium dendrites as follows: In the first stages, the Rh^{3+} ions were reduced by PVP at elevated temperature and nucleated to sub-2-nm seeds (Figure 4a inset, in the white dashed circles). The seeds grew and sprouted in random directions to form rice-shaped or horned particles with a size of ~5 nm or grew by Ostwald ripening and/or overgrowth. Then, maybe the rice-shaped and horned particles continued to overgrow or were attached and aggregated to branched structures (dendrites), with the reaction proceeding until the complete consumption of all rice-shaped and horned particles. A similar formation mechanism was also suggested for other noble metal branched structures such as Pt and Ag.[21,22]

Rhodium Horned Particles, Cubes, and Network-Shaped Wires. The other morphologies of the Rh nanostructure can be produced by replacement of F^- with an equal molar quantity of other halogen anions (Cl^-, Br^-, and I^-). Figure 5a shows that the products are made of predominant particles with sharp horns when the F^- is replaced by Cl^-. However, the size distribution is relatively broad, in the range of 3.0 to 11.0 nm. High-yield nanocubes (> 90% selectivity) were achieved by usage of Br^- (Figure 5b and Figure S2, Supporting Information). Furthermore, the size distribution of Rh nanocubes is very narrow; the average diameter is about 4.8 ± 0.3 nm. The clear lattice fringes of a single particle were observed (Figure 5b, inset). The distance between two lattice

(20) Teng, X.; Liang, X.; Maksimuk, S.; Yang, H. *Small* **2006**, *2*, 249.

(21) Wang, L.; Yamauchi, Y. *J. Am. Chem. Soc.* **2009**, *131*, 9152.

(22) Wang, Y. L.; Camargo, P. H. C.; Skrabalak, S. E.; Gu, H. C.; Xia, Y. N. *Langmuir* **2008**, *24*, 12042.

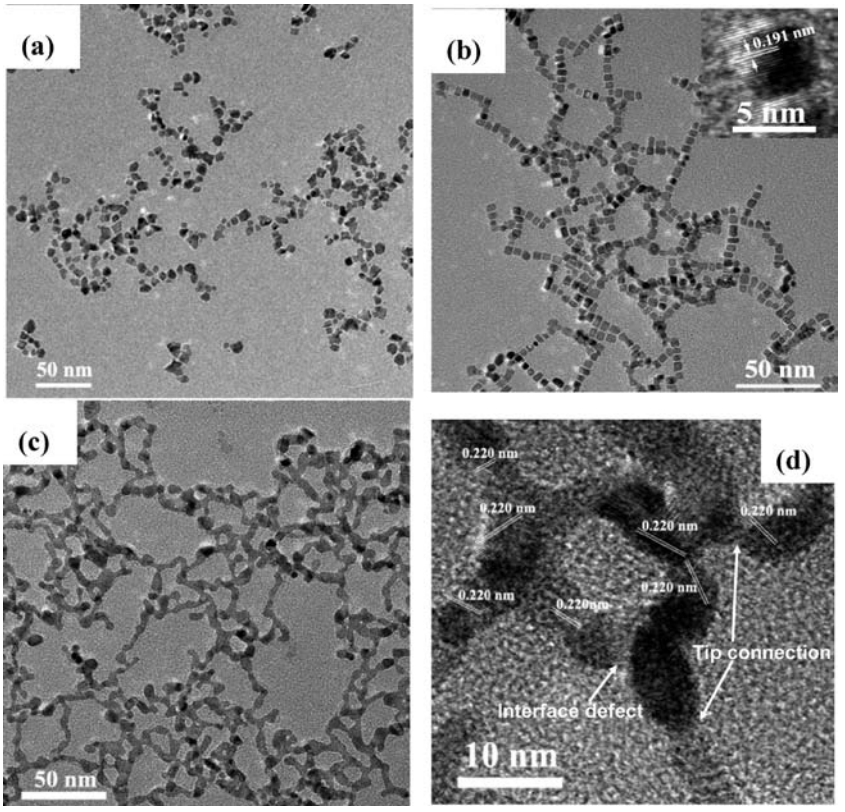

Figure 5. TEM and HRTEM images of other rhodium nanostructures synthesized in the presence of NaCl, NaBr, and NaI. (a) Horned particles, NaCl; (b) cubes, NaBr; (c) and (d) network-shaped wires, NaI.

fringes is approximately 0.191 nm, which is consistent with the interplane distance of the (200) of fcc rhodium. The nanocubes have a strong tendency to self-assemble into a one-dimension linear array because of their small size and uniform shape. Interestingly, when I^- was added into the solution, the high-yield network-shaped wires were obtained (Figure 5c and Figure S3, Supporting Information). The networks were made of different sized, closed, pearl-necklace-shaped loops. The lattice fringes can be observed by HRTEM clearly (Figure 5d). The distance of two lattice fringes is 0.220 nm, which corresponds to the (111) lattice spacing of fcc rhodium. It indicates that the wires were surrounded by {111} planes. The average diameter of the wires is about 5.1 ± 0.3 nm. Furthermore, the pore diameter distribution of networks is very broad, in the range of several nanometers to nearly 100 nanometers (Figure 5c). It implies that networks were formed by random anisotropy growth.

The oriented attachment is a classical formation mechanism suggested to explain the wire-structured formation.[23,24] In our system, the formation mechanism of network-shaped wires is suggested by interface-defect and tip-connection attachment. The existence of interface defects and narrower portions in networks reasonably supported this assumption (Figure 5d). Furthermore, we deduce another factor for the formation of network instead of single wire structures is the presence of a variety of Rh intermediate particles such as rice-, sphere- and triangle-shaped ones (Figure 6). This is the reason why the diameter along the wire direction is not uniform and there are broad and narrow portions in single wires.

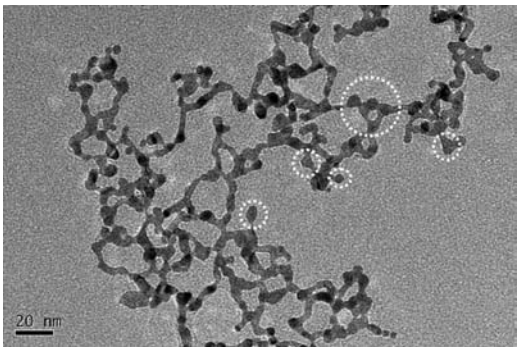

Figure 6. Representative TEM image of network-shaped wires. Note: The shapes in white dashed circles stand for rice-, sphere-, and triangle-shaped particles.

Effects of SLS and Halogen Anions. It is well-known that the size and shape of crystals are mainly controlled by thermodynamic and kinetic factors. The dendritic structure is one of the most complex structures synthesized by the colloidal chemistry process thus far and was produced mainly via kinetic control, because their anisotropic shapes make them possess larger surface areas, which is metastable and energetically unfavorable for thermodynamic control. The sphere particles are often formed by thermodynamic control processes in colloidal chemistry. For obtaining a variety of nonspherical crystal morphologies, inorganic/organic additives were often introduced into the synthesis process to tune the crystal growth through kinetic control. Studies have shown that additives such

(23) Xu, X.; Zhuang, J.; Wang, X. *J. Am. Chem. Soc.* **2008**, *130*, 12527.
(24) Cho, K.; Talapin, D. V.; Gaschler, W.; Murray, C. B. *J. Am. Chem. Soc.* **2005**, *127*, 7140.

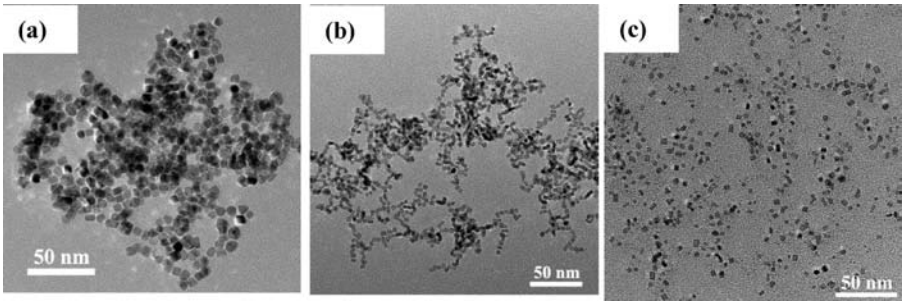

Figure 7. TEM images of rhodium particles synthesized in the absence of SLS. (a) NaCl, (b) NaBr, and (c) NaI.

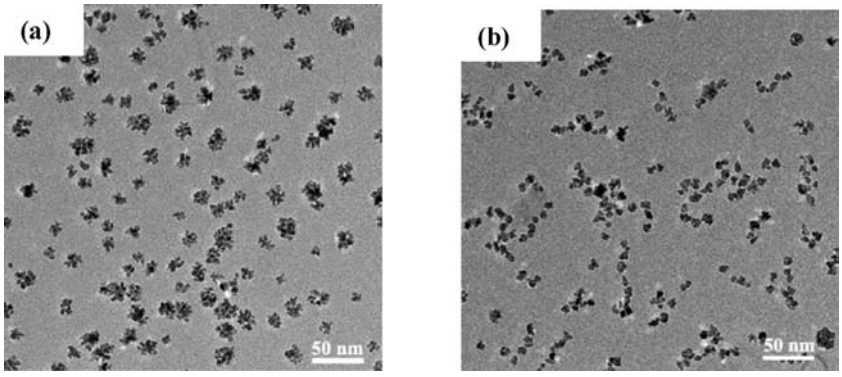

Figure 8. Representative TEM images of Rh nanoparticles synthesized at 220 °C for 6 h by varying the mole ratio of SLS and NaF. (a) SLS/NaF = 4:1 (i.e., SLS, 578 mg; NaF, 21 mg); (b) SLS/NaF = 1:1 (i.e., SLS, 289 mg; NaF, 42 mg).

as Fe^{3+},[25] Ag^{+},[26] Cu^{2+},[27] Cl^{-},[28] Br^{-},[29] I^{-},[30] CTAB,[31] and ligands[32−34] played very important roles in controlling the particle morphology in different synthesis systems. In our present system, it is proposed that the electronegativity and ionic radii of different halogen anions (F^{-}, Cl^{-}, Br^{-}, and I^{-}) should play the most important role in these processes, which would affect the coordination strength/number of rhodium and halogen. Maybe these factors integrate to control the reduction, nuclei, and growth rate of Rh crystals. Furthermore, the effect of SLS is also important in obtaining rhodium crystals with highly selective morphologies. To verify the effect of SLS or halogen anions, the control experiments were investigated in the absence of SLS or halogen anions. As is mentioned above, without halogens, the products consist of ill-defined particles with uncontrollable size (Figure 3b). And without SLS, no Rh crystal products can be obtained in the presence of $RhCl_3$, PVP, and NaF. The size and shape distributions of Rh particles were varied with only the usage of NaCl, NaBr, and NaI (Figure 7). It indirectly proved that SLS would also affect Rh crystal morphology.

In order to further understand the effects of SLS and halogen anions on the morphology of rhodium particles, we took complex rhodium dendrites as an example by varying the molar ratio of SLS and F^{-}. Figure 8a showed that the morphology of rhodium dendrites did not change while increasing the quantity of SLS, but the size distribution was not uniform. However, when the quantity of NaF was decreased, the rhodium dendrites sharply decreased (Figure 8b). The products consisted of predominant irregular particles and a small number of dendrites. And the quantity of branches also sharply decreased. These indicate that the SLS had a predominant effect on rhodium dendrites and also showed that the uniform rhodium dendrites were formed by the synergetic effect of an appropriate ratio of SLS and NaF.

Electrochemical Test toward Ethanol Oxidation. In order to investigate shape-dependent catalytic properties of Rh particles, the typical horn-, cube-, and dendrite-shaped particles were chosen to study their electrocatalytic performances on ethanol oxidation. The electrodes were immersed in a nitrogen-saturated 0.1 M $HClO_4$ solution, and the potential was scanned from −0.28 to 1.0 V (vs SCE) at a scan rate 50 mV/s to obtain the cyclic voltammograms (CVs; Figure 9a). The hydrogen desorption/adsorption electric charges calculated from CVs were used to estimate the electrochemically active surface area (ECSA) of catalysts.[35] The ECSAs of Rh cubes, horned particles, and nanodendrites are 0.78, 0.95, and 1.44 cm^2, respectively. The hydrogen desorption/adsorption peaks locate at different positions owing to the differences of surface atom arrangements originating from a variety of morphologies (Figure 9a). The electrocatalytic

(25) Lim, B.; Lu, X.; Jiang, M.; Camargo, P. H. C.; Cho, E. C.; Lee, E. P.; Xia, Y. N. *Nano Lett*. **2008**, *8*, 4043.
(26) Skrabalak, S. E.; Au, L.; Li, X.; Xia, Y. *Nat. Protoc*. **2007**, *2*, 2182.
(27) Sun, J.; Guan, M.; Shang, T.; Gao, C.; Xu, Z.; Zhu, J. *Cryst. Growth Des*. **2008**, *8*, 906.
(28) Filankembo, S. G. A.; Lisiecki, I.; Pileni, M. P. *J. Phys. Chem. B* **2003**, *107*, 7492.
(29) Yuan, Q.; Zhuang, J.; Wang, X. *Chem. Commun*. **2009**, *43*, 6613.
(30) Millstone, J. E.; Wei, W.; Jones, M. R.; Yoo, H.; Mirkin, C. A. *Nano Lett*. **2008**, *8*, 2526.
(31) Song, J. H.; Kim, F.; Kim, D.; Yang, P. *Chem.—Eur. J*. **2005**, *11*, 910.
(32) Choi, K.-S. *Dalton Trans*. **2008**, 5432.
(33) Kou, X.; Zhang, S.; Yang, Z.; Tsung, C.-K.; Stucky, G. D.; Sun, L.; Wang, J.; Yan, C. *J. Am. Chem. Soc*. **2007**, *129*, 6402.
(34) Xiong, Y.; McLellan, J. M.; Yin, Y.; Xia, Y. *Angew. Chem., Int. Ed*. **2007**, *46*, 790.
(35) Yau, S. L.; Kim, Y. G.; Itaya, K. *J. Am. Chem. Soc*. **1996**, *118*, 7795.

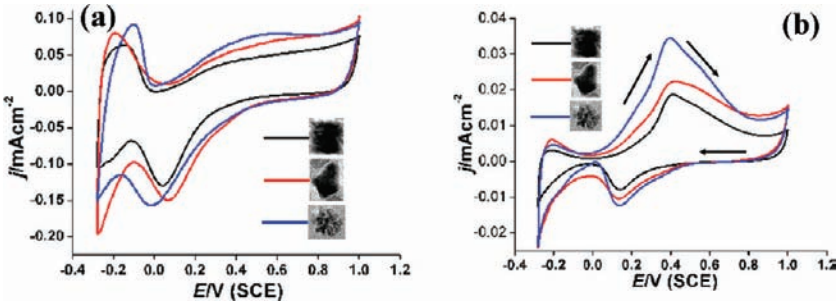

Figure 9. Cyclic voltammetric curves (CVs) of Rh cubes (the black), horned particles (the red), and nanodendrites (the blue). (a) In a 0.1 M $HClO_4$ solution. (b) In a 0.1 M ethanol + 0.1 M $HClO_4$ solution.

activities of catalysts were investigated in the 0.1 M ethanol + 0.1 M $HClO_4$ solution at room temperature (25 °C). The current densities (*j*) were 0.018, 0.022, and 0.035 mA cm^{-2}, which correspond to the cube-, horn-, and dendrite-shaped particles, respectively (Figure 9b). It displayed a shape-dependent catalytic performance, and the catalytic activity enhanced in the order of cube, horn, and dendrite shapes. Among these particles, the Rh nanodentrites have the maximum catalytic activity, which is about 2 times that of nanocubes. It may be ascribed to their maximum ECSA. The enhanced catalytic properties of dendrite-shaped particles were achieved by other research groups.[36,37]

Conclusions

In summary, the highly selective syntheses of Rh nanocrystals with different morphologies such as horned particles, cubes, dendrites, and networks have been achieved through the synergetic effect of SLS and halogen anions (F^-, Cl^-, Br^-, I^-) in an environmentally benign solvent, water, using a one-pot method. In particular, the rhodium nanodendrites and networks were synthesized for the first time. The effects of SLS and halogen anions on rhodium crystal morphology were investigated, and the formation mechanism of rhodium nanostructures is also suggested. This study has demonstrated the successful tuning of the crystal morphology just through utilizing different halogen anions while maintaining other synthetic conditions. The results of electrocatalytic tests toward ethanol oxidation have shown that the Rh nanoparticles displayed shape-dependent properties, and the nanodendrites have the maximum catalytic activity.

Acknowledgment. This work was supported by NSFC (20725102, 20933004 and 20921001), the Fok Ying Tung Education Foundation (111012), Natural Science Foundation of Guizhou Province (20072013), and the State Key Project of Fundamental Research for Nanoscience and Nanotechnology (2006CB932301).

Supporting Information Available: FTIR spectra and large-area TEM images of Rh nanocubes and networks. This material is available free of charge via the Internet at http://pubs.acs.org.

(36) Mahmoud, M. A.; Tabor, C. E.; El-Sayed, M. A.; Ding, Y.; Wang, Z. L. *J. Am. Chem. Soc.* **2008**, *130*, 4590.
(37) Lim, B.; Jiang, M. J.; Camargo, P. H. C.; Cho, E. C.; Tao, J.; Lu, X. M.; Zhu, Y. M.; Xia, Y. N. *Science* **2009**, *324*, 1302.